# Transition state spectroscopy via infrared excitation of LiHF and LiDF van der Waals precursors

Miguel Paniagua, Alfredo Aguado, Manuel Lara, and Octavio Roncero

Citation: J. Chem. Phys. **111**, 6712 (1999); doi: 10.1063/1.480040
View online: http://dx.doi.org/10.1063/1.480040
View Table of Contents: http://jcp.aip.org/resource/1/JCPSA6/v111/i15
Published by the American Institute of Physics.

# Transition state spectroscopy via infrared excitation of Li···HF and Li···DF van der Waals precursors

Miguel Paniagua
*Departamento de Química Física, Facultad de Ciencias C-XIV, Universidad Autónoma de Madrid, 28049 Madrid, Spain*

Alfredo Aguado,[a] Manuel Lara, and Octavio Roncero
*Instituto de Matemáticas y Física Fundamental, C.S.I.C., Serrano 123, 28006 Madrid, Spain*

(Received 27 May 1999; accepted 23 July 1999)

The photoinitiated reactions after infrared excitation from the LiHF and LiDF complexes in the reactant valley are studied as an extension of a recent communication by Paniagua *et al.* [J. Chem. Phys. **109**, 2971 (1998)]. For LiHF two broad bands, associated to $\Delta v=1$ and 2 transitions, are obtained at which the probability of forming LiF products is very high, >90%. For LiDF the $\Delta v=1$ band consists of several narrow resonances, and some of them are supported by the barrier separating reactant and product valleys. Even at these resonances the reaction probability is relatively high, starting at a value about 30% and increasing rapidly to >90% with increasing energy. This implies the tunneling through the barrier. The reason for the high efficiency in the photoinitiated reaction is that the main excitation corresponds to the HF (or DF) stretch within the complex, which is the ''active'' mode for the reaction in agreement with the presence of a late barrier. These results are very different from those obtained in Li+HF or Li+DF collisions at the same total energies, the reaction probabilities being much lower in these latter since the excitation of the HF (DF) mode is unlikely to occur during the collision. © *1999 American Institute of Physics.* [S0021-9606(99)00539-5]

## I. INTRODUCTION

The dynamics near the region of the transition state (TS) determines important features of bimolecular reactions[1] being usually a bottleneck for such processes. Observables obtained in scattering experiments do not provide, however, direct information about the TS due to the average on partial waves. This average often washes out the traces of resonances and any information on transient species appearing in the TS region. In some cases, the resonances associated to these transient states determine the reaction probability.[2] Transition state spectroscopy (TSS) studies provide a more direct information of spectroscopic accuracy on the potential and dynamics of this region where the chemical change of a bimolecular reaction occurs. The information thus obtained is crucial not only to determine the reaction mechanisms but also very useful to control the course of the reaction through the use of well designed excitation pulses.

In TSS studies, the TS region is reached via photon excitation from a specific precursor. This is the case of photodetachment of an electron from a stable negative ion pioneered by Neumark and co-workers,[3–7] or the electronic excitation of van der Waals clusters formed between the reactants. These latter kind of studies are carried out following at least two different alternatives. In the first, developed by Wittig and co-workers,[8–10] one of the molecules forming the van der Waals complex is photodissociated and one of its fragments is ejected towards the second partner. The reaction dynamics in the ground electronic state is then studied under limited geometry conditions imposed by the structure of the initial van der Waals precursor. Since the advent of short laser pulses, this technique has been used to clock bimolecular reactions[11,12] in real time. In the second alternative, one of the partners within the van der Waals complex is promoted to excited electronic states where the whole system reacts, as first done by Soep and co-workers,[13–17] and lately applied by Polanyi and co-workers,[18–20] and González-Ureña and co-workers.[21,22]

The theoretical modeling of this latter kind of TSS studies is particularly complicated nowadays since the reaction dynamics generally involves several excited electronic states, with their mutual nonadiabatic couplings, within spectroscopic accuracy for relatively heavy systems. Just as an example, for the photoexcitation process $Ca(^1S)-HCl \rightarrow \{Ca(^1D,^1P)-HCl\}$ studied by Soep and co-workers,[14–17] the CaCl products are detected not only in the $A\,^2\Pi$ and $B\,^2\Sigma^+$ excited electronic states[14–16] but also in the $X\,^2\Sigma^+$ ground state,[17] which has been found after a careful examination of the highly excited vibrational states of $CaCl(X\,^2\Sigma^+)$. Due to the difficulty of measuring the branching ratio between the different final electronic states of the products, the theoretical study of such processes would be desirable, a difficult task due to the large number of electrons involved. Another good example is Na–HF, recently studied experimentally by Polanyi and co-workers.[20] In this case the Na–HF van der Waals complex, initially in the ground $X\,^2A'$ state, is promoted to the $A\,^2A'$, $B\,^2A''$, and $B'\,^2A'$ electronic states. The spectrum thus obtained[20] is very well reproduced

[a]Present address: Departamento de Química Física, Facultad de Ciencias C-XIV, Universidad Autónoma de Madrid, 28049 Madrid, Spain.

 

in a theoretical simulation by Polanyi, Thrular, and co-workers[23] using potential energy surfaces based on high quality *ab initio* calculations.[24] These excited electronic states present deep wells, and the resonances appearing at low energies decay into the ground electronic state through nonadiabatic couplings. The process has been recently simulated using two coupled energy surfaces within a two degrees of freedom model.[25]

In a recent communication[26] we have shown the possibility of accessing the vicinity of the TS on the ground electronic state via infrared excitation of the Li–HF complex, obtaining a high efficiency in forming LiF products at total energies where the collisional reaction cross-section is rather low. Even though this study was devoted to the particular case of Li–HF, it was discussed that these findings were based on rather general properties of M+HX systems: a sudden change of the electric dipole moment near the TS, and a well in the reactant valley at configurations relatively close to the saddle point. The experimental detection of the products in the photoinitiated reaction of Li–HF presents some disadvantages since this system reacts at thermal energies. However, other related systems like Na–HF (Refs. 24,27,28) and Ca–HF (Ref. 29) have higher reaction thresholds and deep wells in the reactant valley, being thus good candidates for such experiments on the ground electronic state.

Recently, a related experiment has been carried out by Lester and co-workers[30] via a state-selective infrared excitation of the $H_2$–OH complex. The main difference arises from the fact that excitation nearly corresponds to the pure OH overtone. Since the OH is considered to be a ''spectator''[31–33] in the $H_2+OH\rightarrow H_2O+H$ reaction, vibrational excitation does not enhance reactivity, even though the energies considered are well above the reaction barrier. Then, the dominant process is the vibrational predissociation of the complex within the inelastic channel.

In this work we report a detailed description of the photodissociation of the Li–HF and Li–DF complexes when they are promoted via infrared excitation, that is

$$\begin{aligned} \mathrm{Li-HF}+h\nu &\rightarrow \mathrm{Li+HF}(v,j) \quad \text{(inelastic process)} \\ &\rightarrow \mathrm{H+LiF}(v',j') \quad \text{(reactive process)}, \end{aligned} \tag{1}$$

and the same for the deuterated species. The channel for LiH fragments is closed at the energies under study. The infrared excitation mainly affects the HF (or DF) stretch within the complex, what brings the system close to the TS region. The Li+HF potential surface presents a late barrier[34,35] and the reactivity is strongly enhanced by this excitation.[36] Li+HF is not only a prototype for TSS studies in this kind of system but is becoming also a benchmark for theoretical reactive scattering calculations. Its relative low number of electrons allows highly accurate *ab initio* calculations on the ground electronic state[37,38] and recently several global potential energy surfaces (PES) have been published,[34,39] as well as several quantum studies on the reactive collision.[34,35,39–41] In addition, there are molecular beam experiments for HF($v=0$) (Ref. 42) and experiments on the influence of the initial alignment of HF($v=1,j=1$) on the reaction.[43,44] The complementary information obtained in the TSS study presented below is expected to clarify the reactive dynamics in this system.

## II. QUANTUM TIME-DEPENDENT DYNAMICS

In order to obtain the partial cross-sections for the photodissociation of an initial state of the complex, $\Psi_i^{J_i}$ ($J_i$ is the initial angular momentum), to final states of HF ($v,j$) or LiF ($v',j'$) (with total angular momentum $J=J_i,J_i\pm1$) we perform two separated calculations, one using reactant Jacobi coordinates and the second one using product Jacobi coordinates. In reactant Jacobi coordinates, $\mathbf{r}_\alpha$ is the HF internuclear distance, $\mathbf{R}_\alpha$ is the vector joining the HF center-of-mass to the Li atom, and $\gamma_\alpha$ is the angle between $\mathbf{r}_\alpha$ and $\mathbf{R}_\alpha$. In product Jacobi coordinates, $\mathbf{r}_\beta$ is the LiF internuclear distance, $\mathbf{R}_\beta$ is the vector joining the LiF center of mass to the H atom, and $\gamma_\beta$ is the angle between $\mathbf{r}_\beta$ and $\mathbf{R}_\beta$. Since the methodology is analogous in the two sets of coordinates, it will be discussed in terms of generic $\mathbf{r}$ and $\mathbf{R}$ vectors.

It is convenient to use a body-fixed frame, such that the $z$-axis lies along the $\mathbf{R}$ vector and the three atoms lie in the $x$–$z$ plane, to distinguish between the internal coordinates, $r$, $R$, and $\gamma$, and three Eulerian angles $\theta,\phi$, and $\chi$ specifying the orientation of the body-fixed axes with respect to the space-fixed frame.[45] In this representation the total wavepacket is expanded as,

$$\Psi^{JM\epsilon}(\mathbf{R},\mathbf{r},t)=\sum_{\Omega} W_{M\Omega}^{J\epsilon}(\phi,\theta,\chi)\frac{\Phi_{\Omega}^{JM\epsilon}(r,R,\gamma,t)}{rR}, \tag{2}$$

with

$$\begin{aligned} W_{M\Omega}^{J\epsilon}(\phi,\theta,\chi)=&\sqrt{\frac{2J+1}{16\pi^2(1+\delta_{\Omega,0})}}[D_{M,\Omega}^{J*}(\phi,\theta,\chi) \\ &+\epsilon(-1)^{J+\Omega}D_{M,-\Omega}^{J*}(\phi,\theta,\chi)], \end{aligned} \tag{3}$$

where $\epsilon$ is the parity under inversion of spatial coordinates and $D_{M,\Omega}^{J}$ are Wigner rotation matrices[45] corresponding to a total angular momentum $J$. This momentum is associated to the operator $\hat{\mathbf{J}}=\hat{\mathbf{j}}+\hat{\mathbf{l}}$ (with $\hat{\mathbf{j}}$ and $\hat{\mathbf{l}}$ being the angular momentum operators associated to $\mathbf{r}$ and $\mathbf{R}$, respectively). $M$ and $\Omega$ are the projections of the total angular momentum on the space-fixed and body-fixed $z$-axis, respectively. Since the $z$-axis is parallel to $\mathbf{R}$, $\Omega$ is also the projection of the angular momentum of the diatomic fragment.

The integration of the time-dependent Schrödinger equation is accomplished using the Chebyshev method[46] and the $\Phi_{\Omega}^{JM\epsilon}(r,R,\gamma,t)$ coefficients are represented on finite grids for the internal coordinates $r$, $R$, $\gamma$. A set of equidistant points is chosen for the two-dimensional radial grid, and the radial kinetic term is solved using the Fast Fourier Transform method.[47] In order to avoid spurious reflections due to the use of a finite grid, the wavepacket is absorbed after each time step.[48–50] For $\gamma$ we use a DVR representation[51–55] formed by a set of Gauss–Legendre quadrature points, $\gamma_k$, with weights $w_k$. The action of the angular momentum operators on the wavepacket is performed in a single operation as a multiplication of a matrix by a vector as previously explained.[39]

In the framework of first order perturbation theory for electric dipole transitions, the cross-section for excitation of a system from an initial bound state $\Psi_i^{J_i M_i \epsilon_i}$, with energy $E_i$, to the final dissociative states in all the fragmentation pathways is given by[56,57]

$$\sigma(E) \propto \frac{1}{2\pi\hbar}\int_{-\infty}^{\infty} dt e^{iEt/\hbar}\langle \Psi^{JM\epsilon}(\mathbf{R},\mathbf{r},t=0)|\Psi^{JM\epsilon}(\mathbf{R},\mathbf{r},t)\rangle, \tag{4}$$

with $E=E_i+\hbar\omega$ and where the wavepacket at time t=0 is defined as

$$\Psi^{JM\epsilon}(\mathbf{R},\mathbf{r},t=0)=\sum_{\Omega} W_{M\Omega}^{J\epsilon}(\phi,\theta,\chi)\langle W_{M\Omega}^{J\epsilon}|\mathbf{d}\cdot\mathbf{e}|\Psi_i^{J_i M_i \epsilon_i}\rangle. \tag{5}$$

In Eq. (5) **d** is the matrix element of the electric dipole moment in the ground electronic state, whose components are expressed in the body-fixed frame, while **e** is the polarization vector of the incident photon of frequency $\omega$ and defines the orientation of the space-fixed frame. Therefore the transition operator can be written as

$$\mathbf{d}\cdot\mathbf{e}=\sum_{pq}(-1)^p(\mathbf{e})_{-p}D_{pq}^{1*}(\phi,\theta,\chi)d_q(r,R,\gamma). \tag{6}$$

The initial bound state, $\Psi_i^{J_i M_i \epsilon_i}$, is expanded in a basis set as,

$$\Psi_i^{J_i M_i \epsilon_i}=\sum_{vnj\Omega_i\geqslant 0} A_{vnj\Omega_i}^{J_i,\epsilon_i,i}\mathcal{Y}_{j\Omega_i}^{J_i,M_i,\epsilon_i}(\phi,\theta,\chi,\gamma)\frac{\varphi_{vj}(r)}{r}\frac{H_n(R)}{R}, \tag{7}$$

where $\varphi_{vj}(r)$ are the vibrational eigenfunctions of the isolated BC fragment (with eigenvalue $E_{vj}$), $H_n(R)$ are vibrational functions obtained numerically by solving a one-dimension Schrödinger equation with a given reference potential and the angular basis set functions, $\mathcal{Y}$, are defined as

$$\mathcal{Y}_{j\Omega}^{J,M,\epsilon}(\phi,\theta,\chi,\gamma)=\sqrt{\frac{2J+1}{16\pi^2(1+\delta_{\Omega,0})}} \times[D_{M,\Omega}^{J*}(\phi,\theta,\chi)Y_{j\Omega}(\gamma,0) + \epsilon(-1)^J D_{M,-\Omega}^{J*}(\phi,\theta,\chi)Y_{j-\Omega}(\gamma,0)], \tag{8}$$

where $Y_{j\Omega}(\gamma,0)$ is a normalized associated Legendre function.[45,58]

Replacing Eqs. (6) and (7) in Eq. (5), and according to Eq. (2) the coefficients of the initial wave packet become:

$$\Phi_{\Omega}^{JM\epsilon}(R,r,\gamma,t=0)=(-1)^{\Omega}(1-\epsilon\epsilon_i)F_{MM_i}^{JJ_i}(\mathbf{e}) \times\sum_{j\Omega_i\geqslant 0}\sum_q\left[\begin{pmatrix} J_i & 1 & J \\ \Omega_i & q & -\Omega\end{pmatrix} + \begin{pmatrix} J_i & 1 & J \\ \Omega_i & q & \Omega\end{pmatrix}\epsilon(-1)^{J+\Omega}\right] \times\frac{Y_{j\Omega_i}(\gamma,0)d_q(r,R,\gamma)}{2\sqrt{(1+\delta_{\Omega,0})(1+\delta_{\Omega_i,0})}} \times\sum_{vn} A_{vnj\Omega_i}^{J_i,\epsilon_i,i}\varphi_{vj}(r)H_n(R), \tag{9}$$

where it has been used $d_{-q}=(-1)^q d_q$ in the present case. $F_{MM_i}^{JJ_i}(\mathbf{e})$ is related to the polarization function,[45] defined as

$$F_{MM_i}^{JJ_i}(\mathbf{e})=\sum_p(-1)^{M_i}(\mathbf{e})_{-p}\sqrt{(2J+1)(2J_i+1)} \times\begin{pmatrix} J_i & 1 & J \\ M_i & p & -M\end{pmatrix}, \tag{10}$$

where $p=0$ for linearly polarized light (with the $z$ space-fixed axis along the polarization vector of the incident photon) or $p=\pm 1$ for left/right circularly polarized light (with the $z$ space-fixed axis along the direction of propagation of the incident photon).

In each Jacobi coordinate set, the partial cross section for each rovibrational state of the corresponding BC fragment is obtained using the method of Balint–Kurti *et al.*,[59] as

$$\sigma_{vj\Omega}^{BC}(E)=\frac{2\pi k_{vj}(E)}{\mu}|A_{vj\Omega}(R_\infty,E)|^2, \tag{11}$$

where $k_{vj}=\sqrt{2\mu(E-E_{vj})/\hbar^2}$, $\mu$ is the A+BC reduced mass, $R_\infty$ is a large value of the $R$ scattering coordinate such that the interaction between the BC diatomic fragment and A atom is zero, and

$$A_{vj\Omega}(R_\infty,E)=\frac{1}{2\pi}\int_0^\infty dt e^{iEt/\hbar}\langle\varphi_{vj}(r)Y_{j\Omega}(\gamma,0) \times|\Phi_{\Omega}^{JM\epsilon}(R_\infty,r,\gamma)\rangle. \tag{12}$$

[In Eq. (11) there is a difference of 16 $\pi^2$ with respect to the definition made in Ref. 59 arising from a different normalization factor in the asymptotic form of the scattering wavefunction, as has been noted recently.][60]

The overall cross-section in the other rearrangement channel, $\sigma^{\text{no-BC}}$, for each of the two Jacobi coordinates considered, can be obtained analyzing the flux[61] with a method analogous to that applied by Zhang *et al.*,[62] to photopredissociation, in which

$$\sigma^{no-BC}(E)=-i\frac{2\pi}{m}\sum_{\Omega}\int dR\sin\gamma d\gamma\Psi_{\Omega}^{JM\epsilon*} \times(r_\infty,R,\gamma,E)\left.\frac{\partial\Psi_{\Omega}^{JM\epsilon}(r,R,\gamma,E)}{\partial r}\right|_{r=r_\infty}, \tag{13}$$

where $m$ is the BC reduced mass and the time-independent wave function is defined as

$$\Psi_{\Omega}^{JM\epsilon}(r,R,\gamma,E)=\frac{1}{2\pi}\int_0^\infty dt\, e^{iEt/\hbar}\Phi_{\Omega}^{JM\epsilon}(r,R,\gamma,t). \tag{14}$$

These quantities are used to check the accuracy of the calculations since the total absorption cross-section in Eq. (4) can be recalculated as

$$\sigma(E)=\sum_{vj\Omega}\sigma_{vj\Omega}^{\mathrm{BC}}(E)+\sigma^{\mathrm{no-BC}}(E). \tag{15}$$

In addition, we also compare the results obtained in the two possible sets of coordinates, finding an agreement better than 99%, the largest errors occurring only at some energies close to a few resonances or at energies where the absorption spectrum is very small.

The time independent wave functions of Eq. (14) may be used to analyze the nature of the resonances. Assuming the total Hamiltonian as $H=H_0+V$, where $H_0$ has bound zero-order eigenstates, $\phi_n^0$, as well as a continuum of eigenstates, $\phi_{\alpha,E}^0$ (where $\alpha$ denotes a collection of quantum numbers specifying the final state of the fragments and $E$, the total energy), the dissociative eigenstates of $H$ near an isolated resonance can be expressed as a linear combination of the zero-order solutions of $H_0$ as[63]

$$\Psi_\beta(E)=A_n^\beta(E)\phi_n^0+\sum_\alpha\int dE'\,B_{\alpha,E'}^\beta(E)\phi_{\alpha,E'}^0. \tag{16}$$

Therefore, the time-independent wave functions of Eq. (14) contain contributions of the zero-order bound state, the one of interest to assign the resonance, and of continuum solutions, which present oscillations and hide somehow the relevant information searched for. An interesting alternative is that proposed by Sadeghi and Skodje[64] in order to analyze the resonances appearing in the $D+H_2$ collision and also applied to the study of resonances in $F+H_2$.[65] The method combines time-independent wavefunctions for several total energies near the resonance, with a weight function $(E-E_n-i\Gamma_n)^{-1}\propto A_n^{\beta *}(E)$. According to Eq. (14), this is equivalent to use the expression

$$\phi_n^0\approx\mathcal{R}e\int_0^\infty dt e^{i(E_n+i\Gamma_n)t/\hbar}\Psi^{JM\epsilon}(\mathbf{R},\mathbf{r},t), \tag{17}$$

where $E_n$ and $\Gamma_n$ are the approximate position and width of the resonance, respectively. Since the phases of the continuum contributions in Eq. (16) change with total energy, there will be a destructive interference among them, so that the continuum contributions in Eq. (17) are expected to be rather small. However, the discrete function in Eq. (16) does not depend on energy and the square of the $A_n(E)$ shows a near Lorentzian behavior[63] in the vicinity of an isolated resonance. Therefore, its contribution is expected to remain in Eq. (17).

## III. RESULTS AND DISCUSSION

### A. Preliminary considerations and Bound states

One feature of the system under study is the importance of zero-point energy. Considering the potential energy surface the reaction is endothermic but when the zero-point energy of the diatomic fragments is taken into account, the situation is inverted and the reaction becomes exothermic. This is of course due to the fact that the vibrational frequency of LiF ($\approx 900\,\mathrm{cm}^{-1}$) is lower than that of HF ($\approx 4000\,\mathrm{cm}^{-1}$) or DF ($\approx 3000\,\mathrm{cm}^{-1}$). In Table I the vibrational eigenvalues of the diatomic fragments are listed. The energies are referred to the minimum of the isolated HF. In addition, the PES[39] shows a barrier for the reaction with the saddle point placed on the product valley with an energy of $\approx 1880\,\mathrm{cm}^{-1}$. This fact has two major effects. First, the reaction cross-section for the Li+HF($v=0$) or Li+DF($v=0$) collision presents a threshold (in the HF this threshold is due to the zero-point energy at the transition state[39,36]). Second, the reaction is greatly enhanced with the initial vibrational excitation of the reactants.

TABLE I. Vibrational eigenvalues of the isolated diatomic fragments (in $\mathrm{cm}^{-1}$) and effective rotational constants. All energies are referred to the minimum of the isolated HF diatomic molecule.

| | HF | DF | LiF |
|---|---|---|---|
| $v=0$ | 2045.63 | 1486.64 | 1108.50 |
| $v=1$ | 5997.85 | 4386.86 | 1991.74 |
| $v=2$ | 9774.55 | 7194.97 | 2858.29 |
| $v=3$ | 13 374.85 | 9910.72 | 3708.44 |
| $v=4$ | 16 797.44 | 12 533.73 | 4542.49 |
| $v=5$ | 20 040.63 | 15 063.53 | 5360.75 |
| $v=6$ | 23 102.33 | 17 499.54 | 6163.52 |
| $v=7$ | 25 980.03 | 19 841.04 | 6951.14 |
| $B_e$ | 20.74 | 10.90 | 1.31 |

The barrier on the reaction path, responsible for some of these features of the reaction dynamics, appears as a result of a curve crossing. In general, the reactions of M+HX systems are envisaged as harpoon-type processes in which the adiabatic ground electronic state can be understood as the result of a curve crossing between an ionic ($M^+ + HX^-$) and covalent (M+HX) diabatic states. This fact is illustrated for the particular case of the LiHF system in Fig. 1, where some cuts of the PES for the ground (covalent) and the excited (ionic) electronic states are shown as a function of the HF internuclear distance for a collinear Li–F–H configuration and several Li–F distances.[66] It is clearly seen that, as long as Li approaches HF, the ionic state is stabilized with respect to the covalent state and, at a given distance, they cross originating the barrier. At the precise nuclear configuration where the curve crossing occurs, there is a sudden change in the system charge density, as it has been described in detail for Li–HF by Chen and Schaefer[67] and for Ca–HF by Jaffe *et al.*[29] This can be viewed as a charge ''jump'' from the Li to the H atom.

Close to the TS region, there is a well in the reactant valley with a depth of $\approx 2250\,\mathrm{cm}^{-1}$ with respect to the minimum of the isolated HF,[39] in agreement with experimental data obtained from backward glory scattering.[68] This well is already in the Li+HF covalent diabatic electronic state mentioned above,[66] and is due to the interaction between the strong electric dipole of HF and the Li atom. There is a second well in the product valley[39] but less deep and it will be omitted hereafter.

The reactant well presents several bound states, and the first eigenvalues for LiHF and LiDF are listed in Table II. The two systems show different progressions of levels because there is an important reduction of the bending frequency (from $\approx 400$ to $\approx 300\,\mathrm{cm}^{-1}$) when changing from Li–HF to Li–DF, while the stretching frequency is nearly unchanged (being $\approx 350\,\mathrm{cm}^{-1}$). This effect is expected since the kinetic term for the stretching depends on

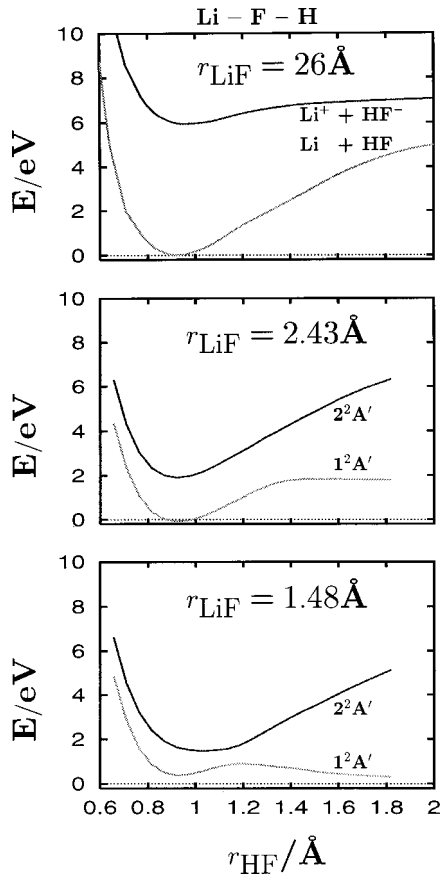


FIG. 1. Cuts of the potential energy surfaces of the ground and first ionic states of Li–F–H, as a function of the HF internuclear distance and at several distances to the Li atom in collinear configuration (Ref. 66).

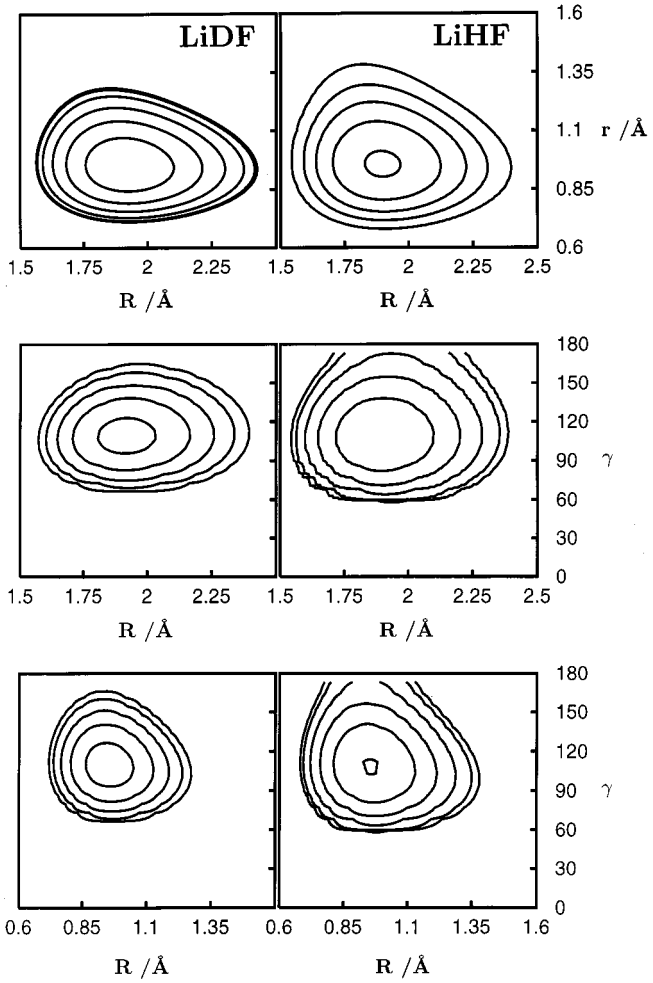


FIG. 2. Contour plots of the probability density associated to the ground van der Waals state of the Li–HF and Li–DF (J=0) as a function of two of the internal reactant Jacobi coordinates and averaging over the third one. Each contour corresponds to a tenth of the preceding one.

$\mu = m_{Li}(m_{H(D)} + m_F)/(m_{Li} + m_{H(D)} + m_F)$ which remains almost equal for both isotopes, while the bending also depends on the HF (or DF) reduced mass, $m = m_{H(D)}m_F/(m_{H(D)} + m_F)$, which nearly increases by a factor of 2. This isotopic effect is even more significant for the HF vibration, and explains why the zero-point energy of the ground state of the complex reduces in about $500\,cm^{-1}$ under isotopic substitution, since the vibrational frequency of HF, $\approx 4000\,cm^{-1}$, reduces to $\approx 3000\,cm^{-1}$ in the DF case.

In this work we shall study the photoinitiated reaction dynamics from the ground van der Waals state (in a $J_i = 1 \rightarrow J = 0$ transition) and in Fig. 2 different contours of the probability density are shown for such levels of LiHF and LiDF. The isotopic effects in LiHF and LiDF are illustrated in Fig. 2, where different contours of the probability density have been plotted in the region where this density is meaningful.

TABLE II. Eigenvalues of Li–HF and Li–DF (in $cm^{-1}$) in the reactant valley well for $J=0$. The approximated quantum numbers $(v,n,b)$ correspond to the HF (or DF) vibration, Li–HF (or Li–DF) vibration and the bending, respectively.

| Li–HF | | Li–DF | |
|---|---|---|---|
| $(v,n,b)$ | Li–HF | $(v,n,b)$ | Li–DF |
| (0,0,0) | −64.24 | (0,0,0) | −590.47 |
| (0,1,0) | 298.93 | (0,0,1) | −288.20 |
| (0,0,1) | 331.65 | (0,1,0) | −230.77 |
| (0,2,0) | 595.67 | (0,0,2) | −36.91 |
| (0,0,2) | 626.99 | (0,1,1) | 38.95 |
| (0,1,1) | 682.21 | (0,2,0) | 81.07 |
| (0,3,0) | 815.47 | (0,0,3) | 155.13 |

### B. Electric dipole moment

The molecular electric dipole moment of the ground electronic state has been calculated with a multiple reference single and double excitations configuration interaction method (MRDCI)[69] using the same basis set functions and configurations as those used to calculate the *ab initio* points.[37] In order to test the quality of the Gaussian basis set, we have calculated the electric dipole moment of the isolated diatomic molecules HF and LiF. The MRDCI calculations[70] yield results in excellent agreement with the best available data. In Fig. 3 (upper panel) we compare the best available data on this magnitude[71,72] with our results for HF ($X^1\Sigma^+$) ground state. With respect to LiF, our results (Fig. 3, lower panel) are very similar to those obtained by Bauschlicher and

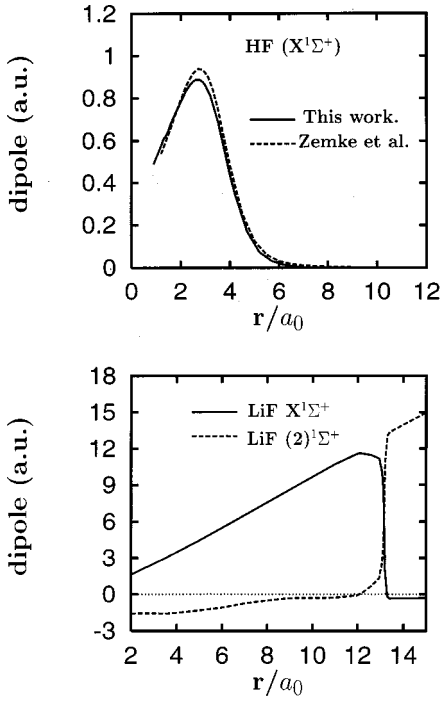


FIG. 3. Calculated electric dipole moments of the HF and LiF diatomic fragments compared to those from Zemke *et al.* (Ref. 71) for HF.

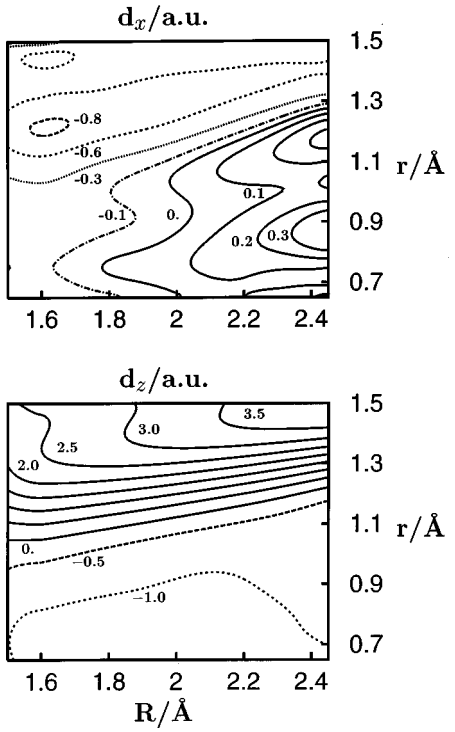


FIG. 4. Components of the electric dipole moment of LiHF on the *x* (a) and *z* (b) body-fixed axes in the reactant Jacobi coordinates.

Langhoff[73] (see Fig. 10 of Ref. 73), showing that the dipole moment function for the two lowest $^1\Sigma^+$ states cross at a distance about 13 $a_0$.

The analytical fit of the two components of the molecular electric dipole moment in the $x-z$ body-fixed plane presents some difficulties because they show a sudden change of sign, as it can be observed for the diatomics in Fig. 3. Such a behavior is due to the curve crossing between the covalent and ionic diabatic states, that strongly depends on the internal variables. For this reason, instead of trying a global fit of the electric dipole components describing the entire configuration space, we have fitted them in the region where the ground state of the reactant complex has a nonnegligible probability density. The molecular dipole moment function of LiHF was calculated on a grid of geometries given by (distances in atomic units)

$$R_{\mathrm{HF}}=1.74+0.1i \quad (i=-5,-4,\ldots,0,\ldots,10,11),$$
$$R_{\mathrm{LiF}}=2.99+0.2j \quad (j=0,\ldots,8), \tag{18}$$
$$\Theta_{\mathrm{LiFH}}=60,\ 71,\ 90,\ 106,\ 135,\ 170,\ \text{and}\ 180\ \text{degrees}.$$

Thus, only 994 of the 3244 calculated points are located in the region of interest. The $d_\alpha(\alpha=x,z)$ Cartesian components of the total dipole moment have been expanded as

$$d_\alpha(R_{\mathrm{HF}},R_{\mathrm{LiF}},\Theta_{\mathrm{LiFH}}) = \sin^l\Theta_{\mathrm{LiFH}} \times\left\{\sum_{ijk}^{M} d_{ijk}\rho_{\mathrm{LiF}}^i\rho_{\mathrm{HF}}^j\rho_{\mathrm{LiH}}^k+T(R_{\mathrm{LiF}},R_{\mathrm{HF}},R_{\mathrm{LiH}})\right\}, \tag{19}$$

with

$$\rho_{AB}=R_{AB}e^{-\beta_{AB}R_{AB}}, \tag{20}$$

$$T(R_{\mathrm{LiF}},R_{\mathrm{HF}},R_{\mathrm{LiH}}) = d_{\mathrm{LiF}}\tanh[\gamma_{\mathrm{LiF}}(R_{\mathrm{LiF}}-R_{\mathrm{LiF}}^e)] + d_{\mathrm{HF}}\tanh[\gamma_{\mathrm{HF}}(R_{\mathrm{HF}}-R_{\mathrm{HF}}^e)] + d_{\mathrm{LiH}}\tanh[\gamma_{\mathrm{LiH}}(R_{\mathrm{LiH}}-R_{\mathrm{LiH}}^e)], \tag{21}$$

and where $l=0$ if $\alpha=x$ and $l=1$ if $\alpha=z$. The out-of-plane *y* component of the molecular dipole moment is zero by symmetry. $R_{\mathrm{HF}}$ is the HF (or DF) internuclear distance, $R_{\mathrm{LiF}}$ is the LiF internuclear distance, and $\Theta_{\mathrm{LiFH}}$ is the angle between these two vectors defined such that the zero value corresponds to a linear F–H–Li configuration. In Eq. (19) a new body-fixed frame has been defined, in which the molecule is also in the $x-z$ plane but the *z*-axis is parallel to the $\mathbf{R}_{\mathrm{HF}}$ vector. The sum has been extended up to $M=6$ for $\alpha=x$ and $M=8$ for $\alpha=z$. Due to the large number of parameters used, they are not listed but can be obtained upon request.

The coordinates and frame have been chosen so that the fit expressed in Eq. (19) is independent of the masses. It is therefore valid for LiHF as well as for LiDF. The electric dipole components of Eq. (19) are transformed to the body-fixed frame associated to the reactant or product Jacobi coordinates used in the dynamical calculations by a rotation around the *y* body-fixed axis, i.e., in the plane of the triatomic system.

In Figs. 4 and 5 we show contour plots of the electric dipole moment components of LiHF in reactant Jacobi coordinates as well as in product Jacobi coordinates, for $\gamma$ corresponding to the minimum of the potential ($\gamma_\alpha=107°$ for reactant Jacobi coordinates and $\gamma_\beta=131°$ for product Jacobi coordinates). The main feature is that in all cases there is a

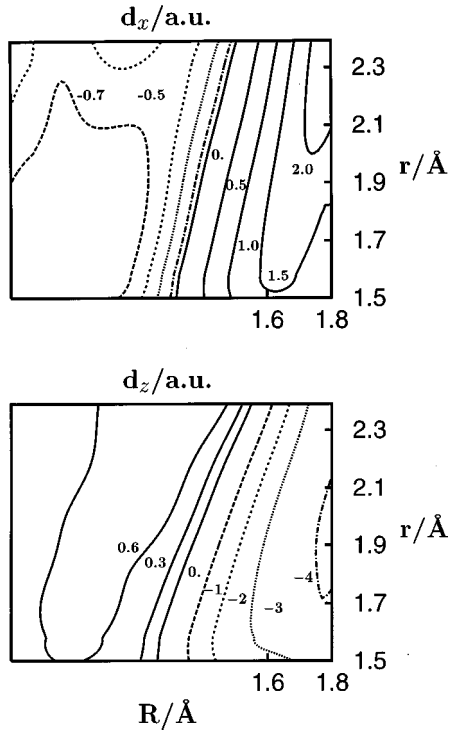


FIG. 5. Components of the electric dipole moment of LiHF on the *x* (a) and *z* (b) body-fixed axes in the product Jacobi coordinates.

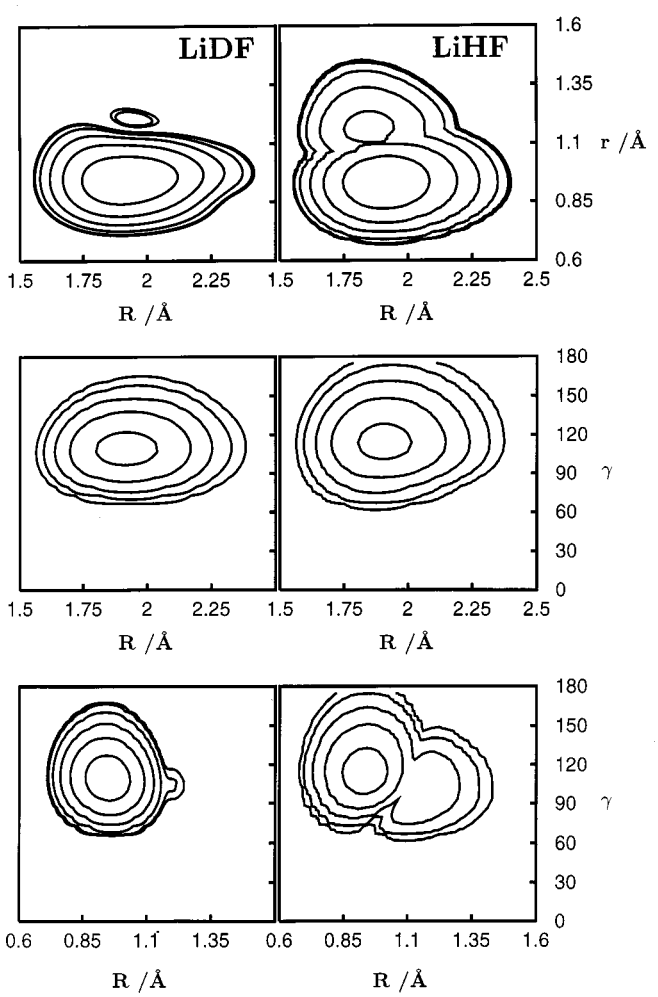


FIG. 6. Contour plots of the probability density associated to the initial wavepacket as a function of two of the internal reactant Jacobi coordinates and averaging over the third one. Each contour corresponds to a tenth of the preceding one.

line at which a sudden change of the dipole originated by the curve crossing is produced. It is also interesting to note that in reactant Jacobi coordinates $d_z$ is much larger than $d_x$, while in product Jacobi coordinates the two components are of the same magnitude. This fact should introduce important differences between the vector properties of the HF and LiF fragments that will be considered in the future.

### C. Dissociation dynamics

The initial wavepacket, in Fig. 6, is built up using Eq. (9) to study the $J=0\leftarrow J_i=1$ transition from the ground bound state of the complex. It shows a node along the *r* reactant Jacobi coordinate describing the HF stretch while it does not seem to have any excitation in the other two coordinates. However, it should be noted that the second maximum in Fig. 6 has much lower probability than the first one, and the initial wavepacket essentially corresponds to $v=0$ in the HF stretching mode. In fact, the square of the overlap of the initial wavepacket with the ground bound level with $J=0$ is $\approx 0.72$ for LiHF, and $\approx 0.98$ for LiDF. Since the main purpose of this work is the study of the fragmentation dynamics, the first seven bound states with $J=0$ are subtracted to the initial wavepacket. After a renormalization, most of the wavepacket fragmentates what reduces numerical errors.

The absorption spectra obtained using Eq. (4) for LiHF and LiDF, in Fig. 7, show different intensities in two energy intervals, one at low energy (between $2500-4000\,\mathrm{cm}^{-1}$ for LiHF and between $1500-3000\,\mathrm{cm}^{-1}$ for LiDF) which essentially corresponds to a $\Delta v=1$ transition in the HF stretch, and a second one at higher energies (between $5000-9000\,\mathrm{cm}^{-1}$ for LiHF and $3500-5500\,\mathrm{cm}^{-1}$ for LiDF) corresponding to the first overtone with $\Delta v=2$. The mean excitation frequencies are smaller than that of the transition in the isolated HF or DF molecules due to the interaction with the Li atom, which weakens the HF bond.

The absorption spectrum for LiDF at lower energies is composed by some resonances [labeled from 1 to 7 in Fig. 7(b)] which have been analyzed using Eq. (17), and the contour plots associated to the probability density are shown in Fig. 8. The continua components are not completely vanished, which introduces a complicated pattern for large internuclear distances in Fig. 8. However, the larger probability contours show a nice structure that can be associated to the zero-order bound states which are responsible for the appearance of the resonances and allows us their assignment (shown in Fig. 8). All of them have one vibrational quantum in the DF stretch while showing a progression in the Li$\cdots$DF stretch and in the bending motion. The two low intensity resonances, the 4th (at $E_4\approx 2367\,\mathrm{cm}^{-1}$) and the 7th ($E_7\approx 2912\,\mathrm{cm}^{-1}$), correspond to (1,0,2) and (1,0,3) vibrations, respectively. The ordering of the assigned levels is the same as those listed in Table II for the bound states with $v=0$. The effective frequency for the bending motion seems to be nearly unchanged while that of the Li–DF stretch becomes

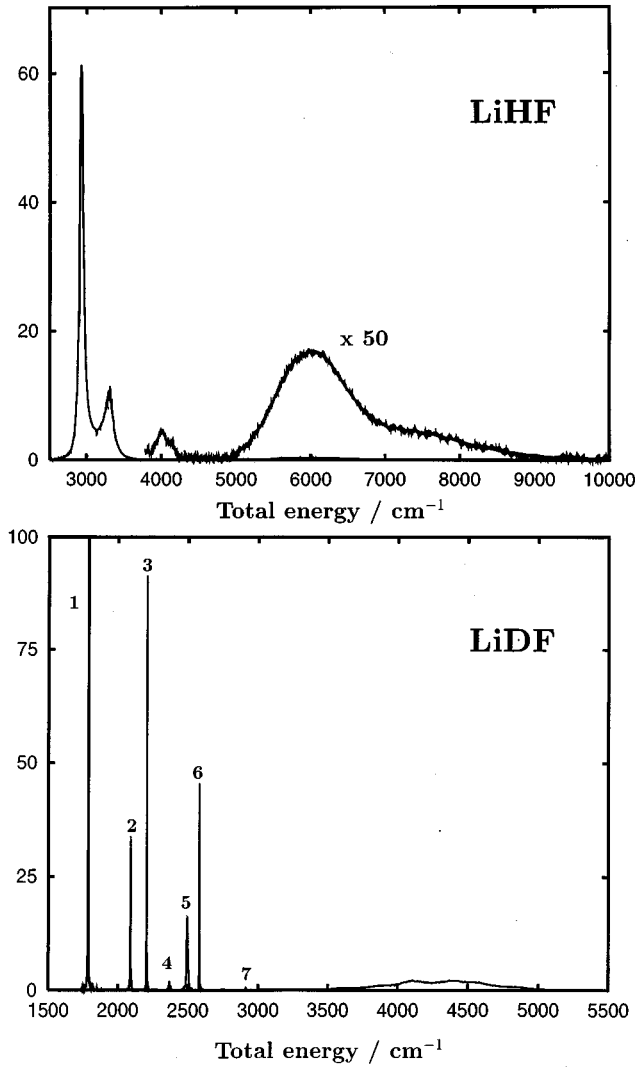


FIG. 7. Absorption spectra for the $J=0\leftarrow J_i=1$ transition from the ground bound states of the LiHF (a) and LiDF (b) complexes. Energy is referred to the minimum of the potential of isolated HF. The photon energy is obtained by adding the energy of the bound state of the complex with $J_i=1$, which is 62.32 and 588.81 cm$^{-1}$, for LiHF and LiDF, respectively. The first resonance for LiDF reaches a value of $\approx$2500 and has been cut to show the other components of the spectrum.

larger in the $v=1$ case. The widths of the resonances do not seem to follow any particular trend either with the increase of total energy or with the selective excitation of a particular vibrational mode. The fragmentation dynamics will be discussed below.

The situation for the $\Delta v=1$ transition in LiHF is, however, very different because in the 2500–4000 cm$^{-1}$ energy range, the spectrum shows a quite broad envelope with two peaks, instead of narrow resonances. The reason is that LiDF is promoted to an energy region close to the saddle point (located at 1879 cm$^{-1}$ as it is shown in Fig. 9) while LiHF is excited well above the top of the barrier, yielding the LiF products with a high probability.[26] The largest frequency of the systems corresponds to the HF (or DF) stretch and this vibrational mode is quite well decoupled from the other two, as demonstrated in the resonance analysis described above. After the infrared excitation to $v=1$, HF starts vibrating without transferring energy to the other internal modes of the system, and the complex fragmentates rapidly since it is above the barrier. Due to the large difference between the H and F masses, the H atom escapes rapidly, leaving the F atom attached to the Li atom. For LiDF, however, the $v=1$ excitation in the DF stretch is supported by the barrier so that the resonances dissociate either to the LiF product channel, by tunneling through the barrier, or to the DF reactant channels by vibrational predissociation.

The photofragmentation of LiHF when excited to $v=1$ and $v=2$ can therefore be considered as a direct dissociation on the products channel.[26] The probability of forming LiF product increases rapidly to a value of approximately 90%–95% for energies below the HF($v=1$) threshold, and is much higher than that corresponding to the same total energies in the Li+HF($v=0$) collision, as shown in Fig. 10. For energies above 5000 cm$^{-1}$, reactivity in the photoinitiated process is about 99%, while that corresponding to the Li+HF($v=1$) collision is of the order of 85%–90% (the $v=1$ threshold is about 6000 cm$^{-1}$). The reaction probability for the Li+HF($v=1$) is, however, comparable to the one associated to the photon excitation in the first band, which is interpreted as an excitation of the HF stretch to $v=1$ within the complex. Therefore, the reaction probability seems to depend mainly on the HF (or DF) vibrational excitation rather than on total energy. The reason for this behavior is that the system presents a late barrier,[74,75] i.e., the saddle point is placed at an internal configuration in which the HF distance is elongated to a large value ($\approx$1.301 Å) as compared to that of the isolated HF ($\approx$0.921 Å). Therefore, to overpass the barrier some vibrational energy is needed in the HF stretching mode, and a single vibrational quantum seems to be enough to produce the reaction with a high efficiency. Such vibrational excitation is easily created by the infrared promotion. However, during the Li+HF($v=0$) collision the HF vibration is not greatly excited and, in order to obtain a high efficiency for the reaction, the HF reactant should be initially in $v=1$, as is shown in Fig. 10.

For the case of Li+HF reactive collision the total reaction cross-sections for HF($v=0,1$, $j=0,1,2$, and 3) have been calculated[36] using a wavepacket treatment in reactant Jacobi coordinates, within the Centrifugal Sudden approach. This approach yields results in very good agreement with exact calculations[39] when considering total reaction probabilities. These calculations show that the reaction cross-section increases by a factor of 10-50 by increasing the vibrational excitation from $v=0$ to $v=1$. This large enhancement of the reaction cross section with initial vibrational excitation of the reagents has been observed experimentally for some related systems, like K+HCl,[76] Ba+HF,[77] Ca+HF,[78,79] Sr+HF,[78–80] and Na+HF.[80] Most of these systems are endothermic for $v=0$, while Li+HF is nearly thermoneutral, but this fact does not seem to make important differences.

It was also found that for Li+HF($v=0,j>0$) the reaction cross section is larger for low $\Omega$, which was taken as an indication that the reaction occurs preferentially at near collinear geometries.[36] This fact was interpreted by assuming that the reaction takes place after some vibrational excitation

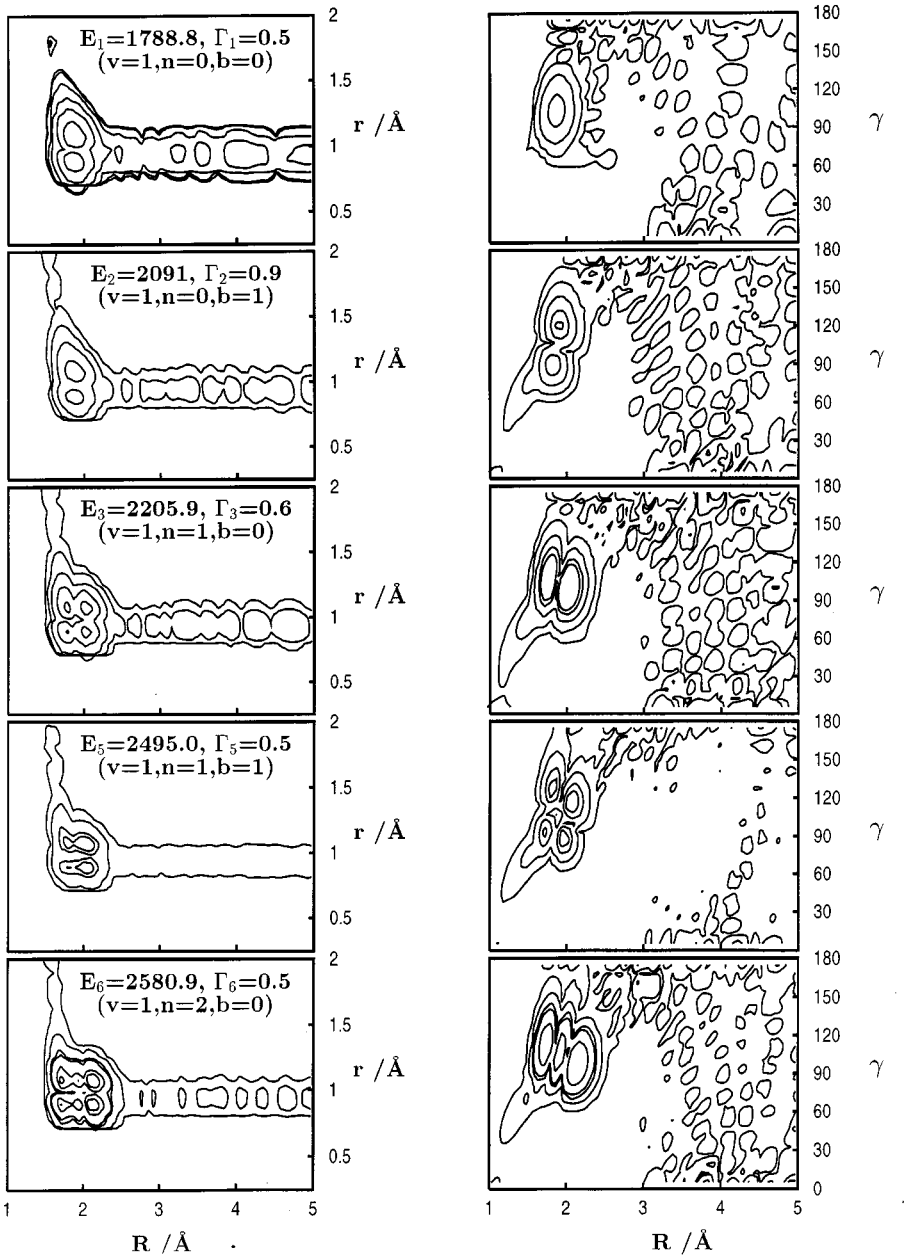


FIG. 8. Contour plots of the probability density associated to the $\phi_n^0$ functions, obtained using Eq. (17), for the five more intense resonances of LiDF as labeled in Fig. 7. The energy position and width are also shown, as well as their assignment.

is gained by the HF fragment during the collision. The efficiency of the vibrational energy transfer is larger at near collinear collisions, which explains why low $\Omega$ give higher reaction cross-sections. Alvariño *et al.*,[81] using the so-called stereodirected representation, found that the reaction probabilities for the Li+HF($J=0$) reaction are larger when the Li atom attacks on the H side of HF, which is in agreement with this model.

The final state distributions of the diatomic fragments after infrared excitation of LiHF complex are shown in Fig. 11 for the first band, i.e., in the 2500–4000 $cm^{-1}$ range. LiF is mainly populated in $v=0$ showing a progressive increase of the population in $v=1$ as the total energy increases. In fact, for the second band at energies larger than 5000 $cm^{-1}$, the LiF products are more vibrationally excited than for the first band. The LiF($v=0,j$) distribution, shown in Fig. 11(b), is nearly independent of the total energy and has a maximum at $j\approx 10$. For LiF($v=1$) products, the rotational distribution looks very similar to that of LiF($v=0$) but with the maximum located at approximately $j=8$. This kind of unstructured final distributions of the LiF products can be expected from a direct photodissociation in which the LiF stretch within the LiFH complex is scarcely excited and acts like a spectator during the dissociation. The rotational distribution of the HF fragments, in Fig. 11(c), shows a structured dependence with total energy. In fact, the total final population of HF has a small background with several narrow structures associated to resonances. At these resonances, the appearance of HF fragments is due to the vibrational predissociation of LiHF from $v=1$.

As discussed above, LiDF exhibits some narrow resonances in the $v=1$ part of the spectrum (for energies below 3500 $cm^{-1}$) and a broad band for $v=2$ at higher energies.

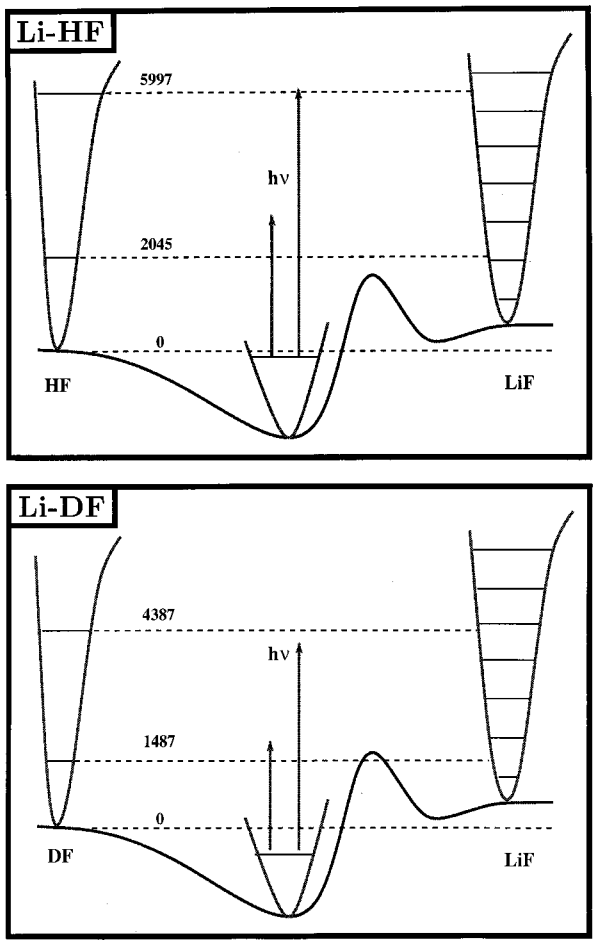


FIG. 9. Energy diagrams for a) LiHF and b) LiDF (all energies are in $cm^{-1}$).

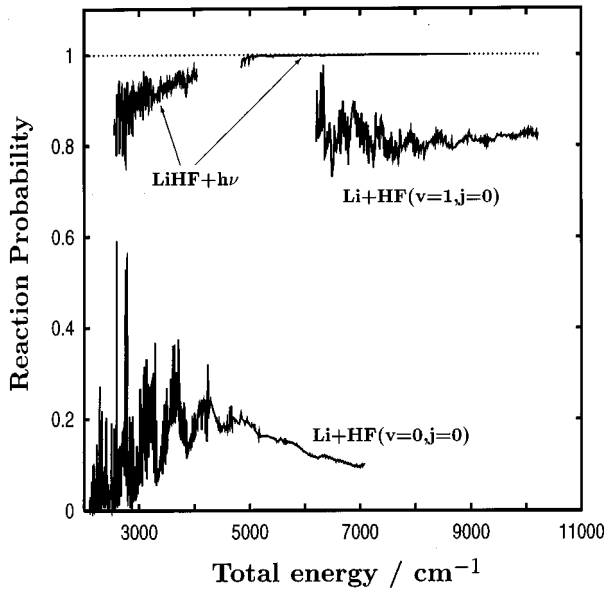


FIG. 10. Reaction probabilities for the two bands of the photoinitiated process in LiHF and for the Li+HF($v=0,1$) collision.

This latter band is well above the barrier for the reaction and may be interpreted, as in the LiHF case, as a direct dissociation towards the LiF product channel. In Fig. 12, the probability of forming LiF products in the photoinitiated process from the LiDF precursor is shown and compared with the corresponding reaction probabilities for the Li+DF($v=0$ and 1) collision. In the whole energy range, the reaction probabil ity after infrared excitation is much higher than that for the Li+DF collision (either $v=0$ or $v=1$). In the photoinitiated process, the reaction probability increases very rapidly with energy and becomes larger than 95% about $3500\,cm^{-1}$. In the collision, however, the reaction probability is always below 40%, even for DF initially in $v=1$.

The reaction probabilities in the collision increase according to the progression DF($v=0$), HF($v=0$), DF($v=1$), and HF($v=1$), i.e., there is an enhancement of the reaction efficiency with the internal vibrational energy of HF or DF listed in Table I. Similar isotopic effects were obtained previously by Laganà *et al.* for the collision, using another PES with a quassiclassical method and a Rotational Infinite Order Sudden Approach.[82]

In the photoinitiated process from LiDF precursor, the efficiency in forming LiF products is also very high, because the infrared promotion mainly excites the DF stretch, as in the LiHF case. There is a fast increase of the reaction probability as soon as the energy is higher than the barrier for the reaction. However, it is notorious that the reaction probability in the first resonance, located at $1788.8\,cm^{-1}$, is of the order of 30%. Since the maximum of the barrier is located at $1879\,cm^{-1}$, the decay of the first resonance in the LiF product channel can only be attributed to tunneling through the barrier. Such high probability for tunneling is only possible because the vibrational predissociation process, LiHF($v=1$)$\rightarrow$Li+HF($v=0$), is rather inefficient, making the competition between the two fragmentation processes possible. The total energies for the remaining resonances in Fig. 7 are above the barrier and the reaction probability increases for them. Therefore, the spectroscopic study of the resonances appearing in the LiDF case provides valuable information about the reaction mechanisms and the potential energy surface below and above the barrier for the reaction.

## IV. CONCLUSIONS

In this work the LiHF photoinitiated reaction in the ground electronic state has been studied, via the infrared excitation of the LiHF precursor (and its deuterated variant), as an extension of a recent communication.[26] In order to simulate the infrared absorption, the electric dipole moment has been calculated using the MRDCI method with the same basis set as previously used to calculate the potential energy surface.[37,39] The electric dipole moment has been fitted to an analytical expression in the region of the well in the Li+HF reactant channel.

The $J=0\leftarrow J_i=1$ transition from the ground state of the reactant complex has been studied using a wavepacket treatment. Two energy intervals can be separated in the absorption spectra, corresponding to $\Delta v=1$ and $\Delta v=2$, respectively. For LiHF it is found that in both cases the probability of forming LiF products is very high, $>90\%$. This result is very different from the corresponding reaction probability in the Li+HF($v=0$) collision at the same total energies, where

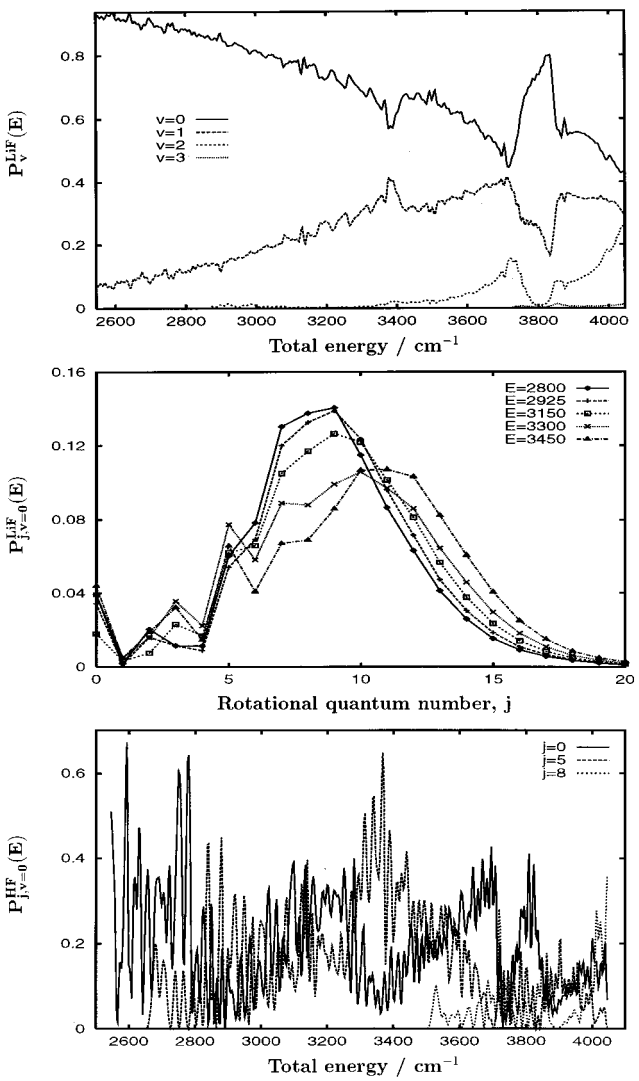


FIG. 11. Final state distribution of the diatomic fragments after infrared excitation of LiHF precursor: (a) LiF vibrational state distribution, (b) rotational distribution of LiF($v=0$) and (c) HF($v=0$) rotational distribution.

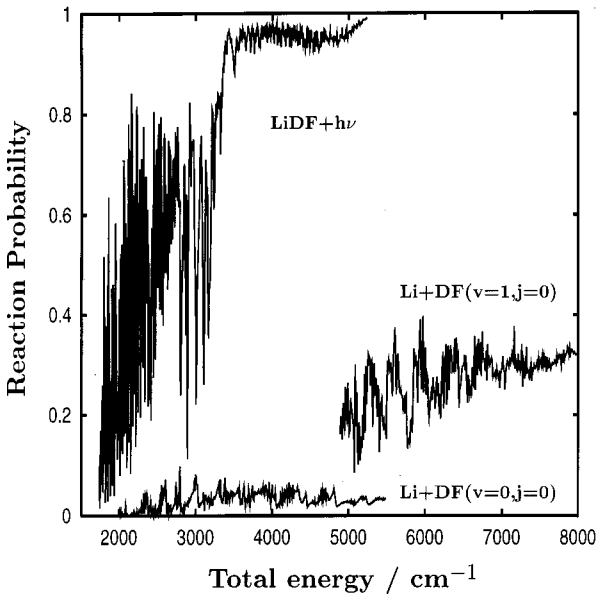


FIG. 12. Reaction probabilities for the photoinitiated process in LiDF and for the Li+DF($v$=0,1) collision.

only a 20% reaction probability is obtained.[39,36] This system has a late barrier and some vibrational excitation is required to overpass it.[36] Thus, the high efficiency of the photoinitiated process is due to the vibrational excitation of the HF stretch produced in the infrared absorption, while in the Li+HF($v=0$) collision vibrational excitation is very unlikely to occur and some initial excitation is required to obtain such an efficiency. The reaction probability for the Li+HF($v=1$) collision is also close to 90%, but this process involves a much higher energy than in the photoinitiated reaction because of the presence of the well in the reactant valley.

The absorption spectrum of LiHF presents broad bands which are interpreted as the result of a direct photodissociation towards the product channel because the excitation energy is above the barrier for the reaction. In the case of LiDF, however, the excitation energy is close to the barrier due to a strong isotopic effect, and the $\Delta v=1$ transition consists of some narrow resonances. It is found that the first resonance is below the barrier and presents a probability of about 30% for the formation of LiF products due to the tunneling through the barrier.

As a conclusion, the photoinduced reaction after infrared excitation of LiHF and LiDF complexes allows the study of the transition state region on the ground electronic state above and below the barrier. Therefore, it provides interesting information about the reaction mechanisms which is complementary to that obtained in the collision between the reactants.

## ACKNOWLEDGMENTS

This work has been supported by DGICYT (Ministerio de Educación y Ciencia, Spain) under Grant Nos. PB97-0027 and PB95-0071, and by the European TMR network Contract No. ERBFMRX-CT96-0088. We also want to acknowledge DGICYT and CIEMAT for the use of a CRAY-J90.

[1] R. D. Levine and R. B. Bernstein, *Molecular Reaction Dynamics and Chemical Reactivity* (Oxford University Press, New York, 1987).
[2] M. I. Hernández, J. Campos-Martínez, P. Villarreal, S. Schmatz, and D. C. Clary, Phys. Chem. Chem. Phys. **1**, 1197 (1999).
[3] R. B. Metz, S. E. Bradforth, and D. M. Neumark, Adv. Chem. Phys. **81**, 1 (1992).
[4] D. M. Neumark, Annu. Rev. Phys. Chem. **43**, 153 (1992).
[5] S. E. Bradforth, D. W. Arnold, D. M. Neumark, and D. E. Manolopoulos, J. Chem. Phys. **99**, 6345 (1993).
[6] E. de Beer, E. H. Kim, D. M. Neumark, R. F. Gunion, and W. C. Lineberger, J. Phys. Chem. **99**, 13627 (1995).
[7] D. M. Neumark, Science **272**, 1446 (1996).
[8] C. Wittig, S. Sharpe, and R. A. Baudet, Acc. Chem. Res. **21**, 341 (1988).
[9] S. K. Shin, Y. Chen, S. Nckolaisen, S. W. Sharpe, R. A. Beaudet, and C. Wittig, Adv. Photochem. **16**, 249 (1991).
[10] R. Liu, A. Kolessov, J. W. Partin, I. Bezel, and C. Wittig, Chem. Phys. Lett. **299**, 374 (1999).
[11] M. Dantus, R. M. Bowman, M. Gruebele, and A. H. Zewail, J. Chem. Phys. **91**, 7437 (1989).
[12] N. F. Scherer, C. Sipes, R. B. Bernstein, and A. H. Zewail, J. Chem. Phys. **92**, 5239 (1990).
[13] C. Jouvet, M. Boivineau, M. C. Duval, and B. Soep, J. Phys. Chem. **91**, 5416 (1987).
[14] B. Soep, C. J. Whitham, A. Keller, and J. P. Visticot, Faraday Discuss. Chem. Soc. **91**, 191 (1991).
[15] B. Soep, S. Abbés, A. Keller, and J. P. Visticot, J. Chem. Phys. **96**, 440 (1992).

[16] A. Keller, R. Lawruszczuk, B. Soep, and J. P. Visticot, J. Chem. Phys. **105**, 4556 (1996).
[17] R. Lawruszczuk, M. Elhanine, and B. Soep, J. Chem. Phys. **108**, 8374 (1998).
[18] K. Liu, J. C. Polanyi, and S. Yang, J. Chem. Phys. **98**, 5431 (1993).
[19] J. C. Polanyi and J-X. Wang, J. Phys. Chem. **99**, 13691 (1995).
[20] X. Y. Chang, R. Ehlich, A. J. Hudson, P. Piecuch, and J. C. Polanyi, Faraday Discuss. **108**, 411 (1997).
[21] S. Skowronek, R. Pereira, and A. González-Ureña, J. Chem. Phys. **107**, 1668 (1997).
[22] S. Skowronek, R. Pereira, and A. González-Ureña, J. Phys. Chem. A **101**, 7468 (1997).
[23] M. S. Topaler, D. G. Truhlar, X. Y. Chang, P. Piecuch, and J. C. Polanyi, J. Chem. Phys. **108**, 5378 (1998).
[24] M. S. Topaler, D. G. Truhlar, X. Y. Chang, P. Piecuch, and J. C. Polanyi, J. Chem. Phys. **108**, 5349 (1998).
[25] Y. Zeiri, G. Katz, R. Kosloff, M. S. Topaler, D. G. Truhlar, and J. C. Polanyi, Chem. Phys. Lett. **300**, 523 (1999).
[26] M. Paniagua, A. Aguado, M. Lara, and O. Roncero, J. Chem. Phys. **109**, 2971 (1998).
[27] M. Paniagua, J. M. García de la Vega, J. R. Alvarez-Collado, J. C. Sanz, J. M. Alvariño, and A. Laganá, J. Mol. Struct. **142**, 525 (1986).
[28] R. Gargano, S. Crocchianti, A. Laganà, and G. A. Parker, J. Chem. Phys. **108**, 6266 (1998).
[29] R. L. Jaffe, M. D. Pattengill, F. G. Mascarello, and R. N. Zare, J. Chem. Phys. **86**, 6150 (1987).
[30] J. M. Hossenlopp, D. T. Anderson, M. W. Todd, and M. I. Lester, J. Chem. Phys. **109**, 10707 (1998).
[31] G. C. Light and J. H. Matsumoto, Chem. Phys. Lett. **58**, 578 (1978).
[32] D. C. Clary, J. Chem. Phys. **95**, 7298 (1991).
[33] D. H. Zhang and J. Z. H. Zhang, J. Chem. Phys. **101**, 1146 (1994).
[34] G. A. Parker, A. Laganà, S. Crocchianti, and R. T Pack, J. Chem. Phys. **102**, 1238 (1995).
[35] A. Aguado, M. Paniagua, M. Lara, and O. Roncero, J. Chem. Phys. **106**, 1013 (1997).
[36] M. Lara, A. Aguado, O. Roncero, and M. Paniagua, J. Chem. Phys. **109**, 9391 (1998).
[37] A. Aguado, C. Suárez, and M. Paniagua, Chem. Phys. **201**, 107 (1995).
[38] H. J. Werner (private communication).
[39] A. Aguado, M. Paniagua, M. Lara, and O. Roncero, J. Chem. Phys. **107**, 10085 (1997).
[40] M. Baer, I. Last, and H.-J. Loesch, J. Chem. Phys. **101**, 9648 (1994).
[41] F. Gögtas, G. G. Balint-Kurti, and A. R. Offer, J. Chem. Phys. **104**, 7927 (1996).
[42] C. H. Becker, P. Casavecchia, P. W. Tiedemann, J. J. Valentini, and Y. T. Lee, J. Chem. Phys. **73**, 2833 (1980).
[43] H. J. Loesch and F. Stienkemeier, J. Chem. Phys. **98**, 9570 (1993).
[44] H. J. Loesch, Annu. Rev. Phys. Chem. **46**, 555 (1995).
[45] R. N. Zare, *Angular Momentum* (Wiley, New York, 1988).
[46] H. Tal-Ezer and R. Kosloff, J. Chem. Phys. **81**, 3967 (1984).
[47] R. Kosloff, J. Phys. Chem. **92**, 2087 (1988).
[48] D. Neuhauser and M. Baer, J. Chem. Phys. **91**, 4651 (1989).
[49] R. S. Judson, D. J. Kouri, D. Neuhauser, and M. Baer, Phys. Rev. A **42**, 351 (1990).
[50] D. Neuhauser and M. Baer, J. Chem. Phys. **92**, 3419 (1990).
[51] J. C. Light, I. P. Hamilton, and J. V. Lill, J. Chem. Phys. **82**, 1400 (1985).
[52] A. C. Peet and W. Yang, J. Chem. Phys. **91**, 6598 (1989).
[53] J. T. Muckerman, Chem. Phys. Lett. **173**, 200 (1990).
[54] G. C. Corey, J. W. Tromp, and D. Lemoine, in *Numerical Grid Methods and Their Application to Schrödinger Equation*, edited by C. Cerjan (Kluwer Academic, Dordrecht, 1993), p. 1.
[55] O. A. Sharafeddin and J. C. Light, J. Chem. Phys. **102**, 3622 (1995).
[56] E. J. Heller, J. Chem. Phys. **68**, 2066 (1978).
[57] E. J. Heller, J. Chem. Phys. **68**, 3891 (1978).
[58] M. Abramowitz and I. A. Segun, *Handbook of Mathematical Functions* (Dover, New York, 1972).
[59] G. G. Balint-Kurti, R. N. Dixon, and C. C. Marston, J. Chem. Soc., Faraday Trans. **86**, 1741 (1990).
[60] S. K. Gray and G. G. Balint-Kurti, J. Chem. Phys. **108**, 950 (1998).
[61] W. H. Miller, J. Chem. Phys. **61**, 1823 (1974).
[62] D. H. Zhang, Q. Wu, and J. Z. H. Zhang, J. Chem. Phys. **102**, 124 (1995).
[63] U. Fano, Phys. Rev. **124**, 1866 (1961).
[64] R. Sadeghi and R. T. Skodje, J. Chem. Phys. **102**, 193 (1995).
[65] C. L. Russell and D. E. Manolopoulos, Chem. Phys. Lett. **256**, 465 (1996).
[66] C. Suárez, A. Aguado, and M. Paniagua, Chem. Phys. **178**, 357 (1993).
[67] M. M. L. Chen and H. F. Schaefer III, J. Chem. Phys. **72**, 4376 (1980).
[68] H. J. Loesch and F. Stienkemeier, J. Chem. Phys. **99**, 9598 (1993).
[69] R. J. Buenker, in *Current Aspects of Quantum Chemistry*, edited by R. Carb (Elsevier, Amsterdam, 1982), Vol. 21.
[70] M. Bettendorff, R. J. Buenker, S. D. Peyerimhoff, and J. Roemelt, Z. Phys. A **304**, 125 (1982).
[71] W. T. Zemke, W. C. Stwalley, S. R. Langhoff, G. L. Valderrama, and M. J. Berry, J. Chem. Phys. **95**, 7846 (1991).
[72] A. Halkier, H. Larsen, J. Olsen, P. Jørgesen, and J. Gauss, J. Chem. Phys. **110**, 734 (1999).
[73] C. W. Bauschlicher, Jr. and S. R. Langhoff, J. Chem. Phys. **89**, 4246 (1988).
[74] J. C. Polanyi and W. H. Wong, J. Chem. Phys. **51**, 1439 (1969).
[75] M. H. Mok and J. C. Polanyi, J. Chem. Phys. **51**, 1451 (1969).
[76] T. J. Odiorne, P. R. Brooks, and J. V. V. Kasper, J. Chem. Phys. **55**, 1980 (1971).
[77] J. G. Pruett and R. N. Zare, J. Chem. Phys. **64**, 1774 (1976).
[78] Z. Karny and R. N. Zare, J. Chem. Phys. **68**, 3360 (1978).
[79] R. Zhang, D. J. Rakestraw, K. G. McKendrick, and R. N. Zare, J. Chem. Phys. **89**, 6283 (1988).
[80] F. E. Bartoszek, B. A. Blackwell, J. C. Polanyi, and J. J. Sloan, J. Chem. Phys. **74**, 3400 (1981).
[81] J. M. Alvariño, V. Aquilanti, S. Cavalli, S. Crocchianti, A. Laganà, and T. Martínez, J. Chem. Phys. **107**, 3339 (1997).
[82] A. Laganà, G. Ochoa de Aspuru, A. Aguilar, X. Gimenez, and J. M. Lucas, J. Phys. Chem. **99**, 11696 (1995).